Journal of Solid State Chemistry 181 (2008) 2814–2827

Contents lists available at ScienceDirect

Journal of Solid State Chemistry

journal homepage: www.elsevier.com/locate/jssc

Electronic and mechanical properties of 5*d* transition metal mononitrides via first principles

Erjun Zhao [a,b], Zhijian Wu [a,*]

[a] State Key Laboratory of Rare Earth Resource Utilization, Changchun Institute of Applied Chemistry, Chinese Academy of Sciences, Changchun 130022, PR China
[b] Graduate School, Chinese Academy of Sciences, Beijing 100049, PR China

ARTICLE INFO

Article history:
Received 9 April 2008
Received in revised form
4 July 2008
Accepted 18 July 2008
Available online 24 July 2008

Keywords:
5*d* transition metal mononitrides
Crystal structure
Formation enthalpy
Elastic constants
Electronic properties

ABSTRACT

The electronic and mechanical properties of 5*d* transition metal mononitrides from LaN to AuN are systematically investigated by use of the density-functional theory. For each nitride, six structures are considered, i.e., rocksalt, zinc blende, CsCl, wurtzite, NiAs and WC structures. Among the considered structures, rocksalt structure is the most stable for LaN, HfN and AuN, WC structure for TaN, NiAs structure for WN, wurtzite structure for ReN, OsN, IrN and PtN. The most stable structure for each nitride is mechanically stable. The formation enthalpy increases from LaN to AuN. For LaN, HfN and TaN, the formation enthalpy is negative for all the considered structures, while from WN to AuN, except wurtzite structure in ReN, the formation enthalpy is positive. The calculated density of states shows that they are all metallic. ReN in NiAs structure has the largest bulk modulus, 418 GPa. The largest shear modulus 261 GPa is from TaN in WC structure. Trends are discussed.

1. Introduction

Due to their unique properties including high hardness, high melting point, good electrical–thermal conductivity, catalytic activity, chemical inertness and superconductivity, the transition metal mononitrides have been studied extensively and used widely in variety of industrial applications, such as hard coatings for cutting tools and magnetic storage devices, diffusion barriers in advanced semiconductor device technologies, generators, maglev trains, optoelectronics and high-power energy industry [1,2]. Till now, there were many studies on transition metal mononitrides. A brief introduction of these studies is given in the following. For 3*d* transition metal mononitrides from ScN to NiN, the structural, electronic and magnetic properties were studied by use of the linear muffin tin orbital (LMTO) method both in rocksalt [3,4] and zinc blende structures [3]. The cohesive properties of 4*d* transition metal mononitrides from YN to PdN in rocksalt structure were studied by use of LMTO method [5]. In addition, a systematic theoretical study of the zinc blende 4*d* transition metal mononitrides from YN to AgN was performed by full-potential linearized augmented-plane-wave (FLAPW) method [6,7]. It was shown that except the insulating YN, all other mononitrides are metallic, and the paramagnetic state was predicted to be stable for the whole series [6,7]. Although there were also many studies on the individual compound on the 3*d* and 4*d* transition metal mononitrides, a detailed description will not be given in this paper since our research focuses on the 5*d* transition metal mononitrides. For the 5*d* transition metal mononitrides from LaN to AuN, many studies were available [8–47,53].

On the experimental side, LaN, HfN, TaN, WN and platinum nitride have been synthesized under different methods. LaN was prepared in the rocksalt structure [8,9]. HfN was grown by zone-annealing technique in the rocksalt structure [10,11], and it was identified as a superconductor [11–13]. The measured bulk modulus of HfN was 306 GPa by neutron scattering measurements [11]. TaN was synthesized in the rocksalt [14–17] and WC (tungsten carbide) structures [17–19] by diverse methods. HfN and TaN thin films were considered to be suitable materials for diffusion barriers in semiconductor technology [20,21]. In addition, TaN film was an attractive interlayer as well as a diffusion barrier layer in $[FeN/TaN]_n$ multilayers for the application as potential write–head material in high-density magnetic recording [22]. WN was synthesized in WC structure in a high-frequency vacuum induction furnace [19]. Recently, platinum nitride was synthesized by laser-heated diamond anvil cell techniques with temperature exceeding 2000 K and pressure around 50 GPa and recovered in zinc blende structure back to ambient conditions. The measured bulk modulus is 372 GPa [23], which was compared to that of cubic boron nitride (cBN). Here, we use the term platinum nitride, instead of PtN. The reason will be given in a later section.

* Corresponding author. Fax: +86 431 8569 8041.
E-mail address: zjwu@ciac.jl.cn (Z. Wu).

0022-4596/$ - see front matter © 2008 Elsevier Inc. All rights reserved.
doi:10.1016/j.jssc.2008.07.022

On the theoretical side, more studies [24–47] were available compared with the experimental studies. For the series from LaN to PtN, the electronic properties in the rocksalt structure were studied by the LMTO method [24,25]. For individual studies, the structure phase stability and superconductivity of LaN was studied by the tight-binding LMTO (TB-LMTO) method within the local density approximation (LDA) [26]. Quite recently, Ciftci et al. [27] have studied the structural, elastic, thermodynamic and electronic properties of LaN by use of the plane-wave pseudopotential (PW-PP) method within the generalized-gradient approximation (GGA). It was found that the phase transition from rocksalt to CsCl structures occurs at the pressure of 25.25 GPa, in consistent with the other theoretical value (26.9 GPa) [26]. In addition, metallic behavior was found for LaN from both the GGA [27,28] and LDA [28] methods. However, the screened-exchange-LDA (sX-LDA) predicted LaN to be a semiconductor with an indirect gap of 0.75 eV [28]. Studies on the electronic structure of HfN have been reported by use of the FLAPW method within GGA and LDA [28], relativistic Korringa, Kohn and Rostoker (KKR) method [29], FLAPW plus local orbitals (FLAPW+lo) method within GGA [30], and density-functional perturbation theory (DFPT) [31]. The mechanical properties have been investigated for HfN in the rocksalt structure [11,28,30–33]. HfN exhibited the strongest anisotropy in IVB transition metal mononitrides, which originated from the strong covalent bonding between metal and nitrogen atoms along $\langle 100 \rangle$ direction [32]. It has been found that a transition from rocksalt to CsCl structure occurs at the pressure of 130 GPa [33]. In rocksalt structure, HfN was found to be a superconductor with the superconducting temperature of 8.9 K [34], in excellent agreement with the experimental value of 8.83 K [13]. The lattice dynamics for the early 5*d* transition metal mononitrides (HfN, TaN and WN) has been studied by the ultrasoft pseudopotential (US-PP) method within GGA [35]. It showed that the rocksalt TaN and WN were predicted to be dynamically unstable, while HfN with rocksalt structure and WN with WC structure were dynamically stable [35]. The superconductivity in HfN is directly related to the anomalies in the phonon spectra which in turn are connected to the number of valence electrons [34,35]. For TaN in the rocksalt structure, the electronic structure and physical properties were studied by diverse theoretical methods, for instance, FLAPW method within GGA and LDA [28], KKR method [29], DFPT [30], US-PP method within GGA [35], FLAPW+lo method within GGA [36], and augmented-plane-wave (APW) method within Hedin–Lundqvist (HL) [37]. In addition, the electronic and elastic properties have been reported for WN [37,38], ReN [38] and OsN [38,39]. Among these nitrides, rocksalt ReN has the largest bulk modulus (396 GPa) [38].

As mentioned earlier, platinum nitride has been recently synthesized [23]. Initially, it was suggested that platinum nitride has the stoichiometry 1:1, i.e., PtN, and crystallized in zinc blende structure. This has triggered extensive theoretical studies on the physical properties of PtN in diverse structures including zinc blende structure [40–47]. The detailed studies showed that PtN underwent a phase transition from zinc blende to rocksalt structure [41,42,46]. The study on PtN with zinc blende, rocksalt, caesium chloride (CsCl) and wurtzite structures revealed that wurtzite structure was the most stable structure and predicted to transform to rocksalt structure at 41.4 GPa pressure [47]. In addition, it was found that zinc blende PtN is mechanically unstable [43–45], and its bulk modulus [41–44,46,47] is only half of the experimental value 372 GPa [23]. Thus, it casts doubt on the stoichiometry of platinum nitride. On this background, platinum nitride with stoichiometry 1:2, i.e., PtN_2, was studied. From theoretical studies, it was found that PtN_2 is mechanically stable in fluorite [48] and pyrite [49,50] structures, and pyrite PtN_2 is energetically more stable than the fluorite one [49,50]. In pyrite structure, its bulk modulus (312 GPa) is comparable with that of experiment (372 GPa) [23], larger than 290 GPa of fluorite structure [48]. Almost at the same time, PtN_2 with pyrite structure was synthesized by Crowhurst et al. [51], and they confirmed the results from the previous theoretical studies that the stoichiometry of platinum nitride is 1:2, and pyrite structure is the most stable phase for PtN_2 [49,50,52]. Nonetheless, the theoretical studies on PtN in diverse structures [40–47] would provide useful references for the current study. Finally for AuN, the structural stability and electronic properties have been investigated by use of the FLAPW+lo method within the GGA and LDA methods, in which the rocksalt structure was the ground state among zinc blende, rocksalt, CsCl and wurtzite structures [53].

Since the superior mechanical properties of the mononitrides are closely related to the electronic structure, in this paper, the physical properties of 5*d* transition metal mononitrides from LaN to AuN are studied by use of the density-functional theory. The general trends are discussed and they might be important for designing new materials. For each nitride, six structures are considered, i.e., rocksalt, zinc blende, CsCl, wurtzite, NiAs and WC.

2. Computational method and crystal structure

All the calculations conducted in this paper were performed within the CASTEP code [54], based on the density-functional theory. The code is suitable for calculations using periodic boundary conditions to infinite lattice system. The Vanderbilt US-PP [55], which describes the interaction of valence electrons with ions, was used with the same cutoff energy of 600 eV. The *k*-points of $8 \times 8 \times 8$ for *Fm*-3*m* (rocksalt) and *F*-43*m* (zinc blende), $16 \times 16 \times 16$ for *Pm*-3*m* (CsCl), $10 \times 10 \times 5$ for $P6_3mc$ (wurtzite), $9 \times 9 \times 6$ for $P6_3/mmc$ (NiAs) and $12 \times 12 \times 11$ for *P*-6*m*2 (WC) are generated using the Monkhorst–Pack scheme [56]. The exchange and correlation functional were treated by the generalized-gradient approximation (GGA-PBE) [57]. Formation enthalpy was calculated from $\Delta H = E(MN) - E(\text{solid } M) - \frac{1}{2}E(\text{solid } N_2)$ at 0 K. The solid molecular N_2 is from its α phase [58]. Lattice parameters and atomic positions were optimized simultaneously. For the self-consistent field iterations, the convergence tolerance for geometry optimization was selected as the difference in total energy, the maximum ionic Hellmann–Feynman force, the stress tensor, and the maximum displacement being within 5.0×10^{-6} eV/atom, 0.01 eV/Å, 0.02 GPa, and 5.0×10^{-4} Å, respectively. The calculated bulk modulus *B* and shear modulus *G* were from the Voigt–Reuss–Hill approximations [59–61]. Young's modulus *E* and Poisson's ratio *v* are obtained by the following formulas:

$$E = 9BG/(3B + G)\ v = (3B - 2G)/[2(3B + G)]$$

In our calculation, GGA method is used. It is known that in GGA, besides LDA formulation, density gradient is included in the GGA formulation. Therefore, it is not surprising that different formation enthalpy is obtained by the two methods. Thus, in the following paper, comparison will only be made with the results from experiments and other GGA calculations; LDA results will be shown as a reference. From previous studies on the 3*d*, 4*d* and 5*d* early transition metal mononitrides, it is known that GGA method gives better results than LDA method, and both methods give the same trends [28].

The considered crystal structures are shown in Fig. 1. In the well-known rocksalt structure, each *M* atom is coordinated by six nitrogen atoms and forms the MN_6 octahedron. The MN_6 octahedra are edge shared. In zinc blende structure, *M* atom is tetrahedrally coordinated by four nitrogen atoms. The MN_4 tetrahedra are corner shared. In CsCl structure, *M* atom is at the

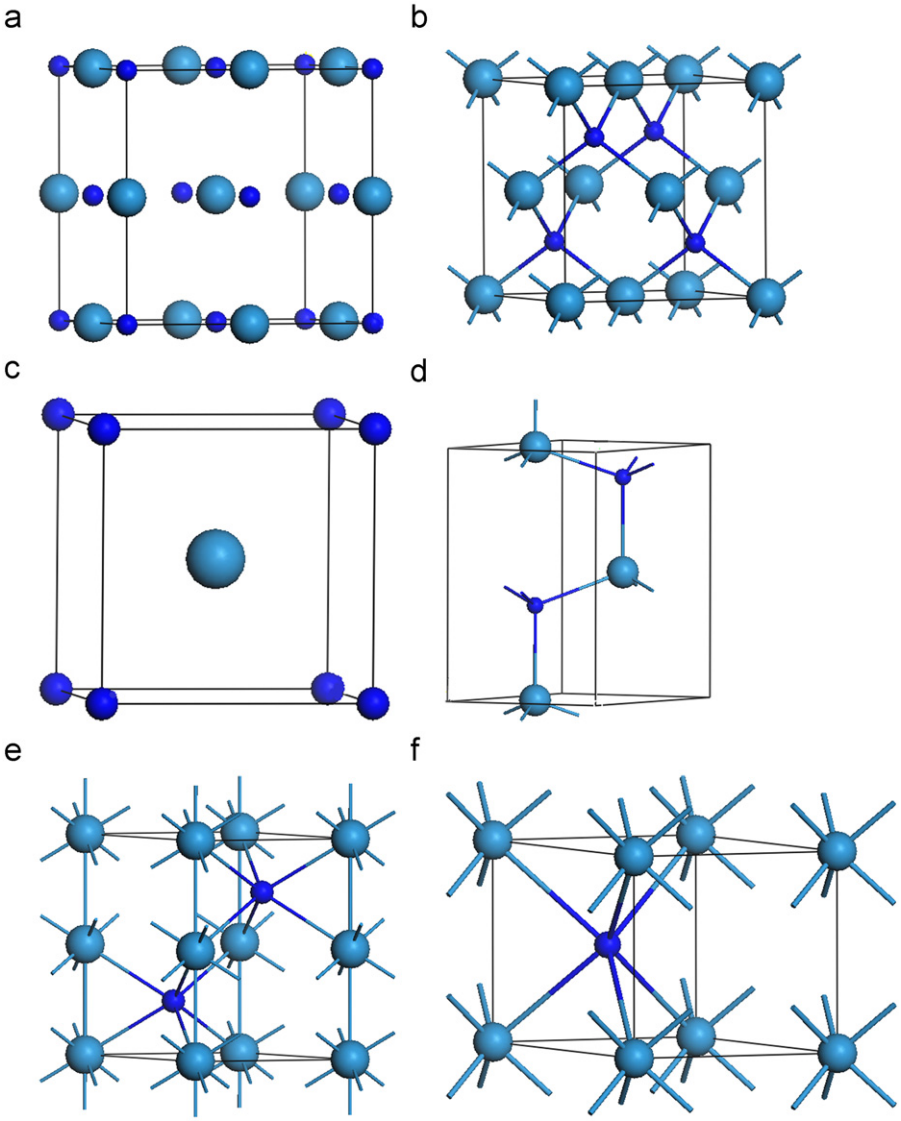

Fig. 1. (Color online) Crystal structures of *M*N (*M* = La–Au): (a) rocksalt, (b) zinc blende, (c) CsCl, (d) wurtzite, (e) NiAs, and (f) WC like. The large (cyan) and small (blue) spheres represent 5*d* transition metal and nitrogen atoms, respectively.

body-centered-cubic position, while the nitrogen atoms occupy the eight corner sites. Both *M* and N atoms are eightfold coordinated. In the wurtzite structure, similar to zinc blende structure, *M* atom is surrounded by four nitrogen atoms, and nitrogen atom is fourfold coordinated by *M* atoms. The MN_4 tetrahedra are also corner shared. In the NiAs structure, each *M* atom is surrounded by two *M* and six nitrogen atoms, and N atom is coordinated by six metal atoms. In WC structure, the *M* atom is located at the center of a trigonal prism formed by nitrogen atoms, and nitrogen has the six nearest *M* neighbors. From the fractional coordinates, it is known that in WC, W is in (0, 0, 0), C is in (1/3, 2/3, 1/2); while in NiAs structure, Ni is in (0, 0, 0), As is in (1/3, 2/3, 1/4). Therefore, it is clear that for each unit cell, NiAs contains the two units (double in *z* direction) of the WC structure.

3. Results and discussion

The calculated lattice parameters and elastic stiffness constants from LaN to AuN are listed in Tables 1–9. For the mechanically unstable structures, their elastic stiffness constants were not presented. Besides the nitrides, the calculated lattice parameters and elastic stiffness constants of the pure metals from their ground state structures are also listed for comparison [62–67]. In order to show the trends of *M*N (*M* = La–Au) compounds, the calculated *M*–N bond distance, cell volume per formula unit, bulk modulus and formation enthalpy per formula unit from LaN to AuN are also sketched in Fig. 2. The total and partial density of states (DOS) for rocksalt structure are shown in Fig. 3.

3.1. Lattice parameters and elastic properties for each nitride

LaN: From Table 1, it is seen that many investigations were available for rocksalt structure. The calculated formation enthalpy is −2.68, 0.44 eV greater than the experimental value −3.12 eV [68]. In addition, our calculated value is also different from those obtained by LDA method, i.e., −3.77 eV [26] and −3.20 eV [28]. In particular, at CsCl structure, LDA method gives a formation enthalpy −3.42 eV [26], differing significantly from −1.21 eV from our GGA calculation. These deviations in theoretical calculation are mainly caused by the different methods as mentioned earlier. Among the considered structures, all of them are thermodynamically stable by the GGA method due to the negative formation

Table 1
LaN

	NaCl *Fm*-3*m* rocksalt	ZnS *F*-43*m* zinc-blende	CsCl *Pm*-3*m*	ZnS $P6_3mc$ wurtzite	NiAs $P6_3/mmc$	WC *P*-6*m*2	hcp La
ΔH	−2.68 −3.12[a], −3.77[b], −3.20[c]	−2.55	−1.21 −3.42[b]	−2.66	−2.03	−2.01	
a	5.348 5.163[b], 5.27[c], 5.293[d] 5.32[e], 5.302[f], 5.295[g], 5.307[h], 5.638[i]	5.688	3.237 2.970[b] 3.167[h]	4.197	3.693	3.612	3.77[d]
c				5.932	6.516	3.293	12.266[d]
V	38.2	46.0	33.9	45.2	38.5	37.2	
La–N	2.674 2.560[b]	2.463	2.803 2.572[b]	2.470	2.683	2.657	
C_{11}	221 213[h]	110	286 315[h]		223		88[j]
C_{33}					310		56[j]
C_{44}	75 71[h]	43	−69 81[h]		23		15[j]
C_{12}	62 84[h]	79	24 164[h]		75		37[j]
C_{13}					30		13[j]
B	115 152[b], 173[c], 120[d] 148[e], 116.947[h]	90	111 282[b] 114.18[h]	91	114	106	36[j] 22[d]
G	77 64.464[h]	28			53		47[j]
E	188 170.88[h]	77			137		101[j]
v	0.23 0.2505[h]	0.36			0.30		0.07[j]

Calculated formation enthalpy per formula unit ΔH (eV), lattice parameters *a* and *c* (Å), cell volume per formula unit *V* (Å^3), the shortest La–N bond distance (Å), elastic stiffness constants C_{ij} (GPa), bulk modulus *B* (GPa), shear modulus *G* (GPa), Young's modulus *E* (GPa), Poisson's ratio *v* at the GGA level for LaN from various space groups: cubic (F*m*-3*m*, no. 225; *F*-43*m*, no. 216; *Pm*-3*m*, no. 221) and hexagonal ($P6_3mc$, no. 186; $P6_3/mmc$, no. 194; *P*-6*m*2, no. 187) phases. Comparison has been made with both experimental and previous theoretical data. Data for elemental La at hexagonal close packed (hcp) phase were also presented.

[a] Ref. [68], experiment.
[b] Ref. [26], TB-LMTO method within LDA.
[c] Ref. [28], FLAPW method within LDA.
[d] Ref. [35], US-PP within GGA.
[e] Ref. [28], FLAPW method within GGA.
[f] Ref. [8], experiment.
[g] Ref. [9], experiment.
[h] Ref. [27], PW-PP method within GGA.
[i] Ref. [69], experiment.
[j] Present work, the *B*, *G*, *E*, *v* values are calculated from the Voigt–Reuss–Hill approximations based on the elastic stiffness constants.

enthalpy. Rocksalt structure is the most stable, followed by wurtzite and zinc blende structures. This indicates that all the considered structures can be synthesized at ambient conditions, although only rocksalt structure was synthesized up to now [8,9,69]. The calculated lattice parameter 5.348 Å for rocksalt LaN deviates by 1% from the early experimental values 5.302 Å [8] and 5.295 Å [9]. However, compared with the recent experimental value 5.638 Å [69], the deviation is large and reaches to 5%. Compared with the previous theoretical values 5.293 Å [35], 5.32 Å [28] and 5.307 Å [27] from the GGA method, our result 5.348 Å matches them within 1%. For CsCl structure, our calculated lattice parameter 3.237 Å matches 3.167 Å [27] from the recent study with the GGA method within 2%.

For rocksalt, zinc blende and NiAs structures, the calculated elastic stiffness constants (Table 1) indicate that they are mechanically stable because they satisfy the elastic stability criteria [70]. In rocksalt structure, the calculated elastic stiffness constants, bulk modulus, shear modulus, etc., are in excellent agreement with the recent theoretical study by the GGA method [27]. From the calculated DOS (Fig. 3), it is seen that LaN in rocksalt structure is metallic due to the finite DOS at the Fermi energy level, in agreement with the calculation by both GGA and LDA methods [28]. This also agrees with the recent GGA calculation [27]. Nonetheless, the sX LDA method [28] predicted that LaN is a semiconductor with a band gap 0.75 eV. In addition, ScN [4,28] and YN [5,28] were also predicted to be semiconductors. This might suggest that further study, in particular experimental ones, are necessary to elucidate the conducting properties of rocksalt LaN.

For CsCl structure, from Table 1, it is noted that it is mechanically unstable from our calculation due to the negative C_{44} value (−69 GPa). However, the recent study by Ciftci et al. [27] with the GGA method predicted that it is mechanically stable with the C_{44} value 81 GPa. So, further study is necessary to solve the discrepancy.

Compared with the pure metal La, the mechanically stable structures, i.e., rocksalt, zinc blende and NiAs, have the bulk modulus around 111 GPa, much larger than 36 or 22 GPa [35] for La. This suggests that the insertion of nitrogen into the La lattice enhances the bulk modulus significantly.

HfN: All the considered structures are thermodynamically stable from their negative formation enthalpy (Table 2), in which rocksalt structure is the most stable, followed by NiAs and zinc blende structures. This indicates that they can be synthesized at ambient conditions, although experimental study was only available for rocksalt structure [10–12]. For rocksalt structure, the calculated formation enthalpy −3.11 eV deviates by 1.02 eV from the LDA result −4.13 eV [28]. The calculated lattice parameter 4.627 Å deviates by around 2% from the experimental value 4.525 Å [10,12], and from previous theoretical calculations [28–30,32,34,35,71]. The calculated elastic stiffness constants are also comparable to both experiment and previous theoretical

Table 2
HfN

	NaCl *Fm*-3*m* rocksalt	ZnS *F*-43*m* zinc-blende	CsCl *Pm*-3*m*	ZnS $P6_3mc$ wurtzite	NiAs $P6_3/mmc$	WC *P*-6*m*2	hcp Hf
ΔH	−3.11 −4.13[a]	−2.53	−1.27	−2.18	−2.53	−2.46	
a	4.627 4.48[a], 4.525[c,d], 4.518[e] 4.54[f,g,h], 4.539[i], 4.53[j] 4.47[k], 4.519[l]	5.020	2.873	3.538	3.191	3.150	3.19[b]
c				5.863	5.801	2.958	5.05[b]
V	24.8 23.3[m], 22.0[n]	31.6	23.7	31.8	25.6	25.4	
Hf–N	2.314 2.263[d]	2.174	2.488	2.177	2.345	2.344	
C_{11}	628 597[i], 664[j], 679[m] 694[n,p], 566[q]	303	518	255	394	440	188.1[o]
C_{33}				261	425	645	196.9[o]
C_{44}	105 118[i], 154[j], 150[m] 134[n], 135[p], 139[q]	77	14	38	122	103	55.7[o]
C_{12}	95 121[i], 115[j], 119[m] 112[n,p], 139[q]	163	117	153	102	172	77.2[o]
C_{13}				169	231	109	66.1[o]
B	272 320[a], 278[f], 269[g,h] 279.8[i], 284[j], 303[k] 276[l], 306[m,n,p], 344[r]	210	251	194	247	253	110[s] 109[b]
G	155	74	55	44	116	137	57[s]
E	390	198	155	123	303	349	147[s]
v	0.26	0.34	0.40	0.39	0.30	0.27	0.28[s]

For detailed expressions, see Table 1.
[a] Ref. [28], FLAPW method within LDA.
[b] Refs. [62,63], experiment.
[c] Ref. [10], experiment.
[d] Ref. [12], experiment.
[e] Ref. [29], KKR method.
[f] Ref. [28], FLAPW method within GGA.
[g] Ref. [34], US-PP within GGA.
[h] Ref. [35], US-PP within GGA.
[i] Ref. [32], US-PP within GGA.
[j] Ref. [30], FAPW+lo method within GGA.
[k] Ref. [71], PP within LDA.
[l] Ref. [71] in Ref. [16], experiment.
[m] Ref. [11], experiment.
[n] Ref. [11], US-PP within LDA.
[o] Ref. [64], experiment.
[p] Ref. [31], DFPT.
[q] Ref. [33], two-body interionic potential theory.
[r] Ref. [13], experiment.
[s] Present work, calculated from the Voigt–Reuss–Hill approximations based on the elastic stiffness constants.

studies (for comparison, see Table 2). In addition, all the considered structures are mechanically stable since the calculated elastic stiffness constants satisfy the mechanical stability criteria [70]. Compared with the pure metal Hf, calculated bulk modulus and shear modulus are much larger than those from hexagonal close-packed (hcp) Hf (110 and 57 GPa, respectively), in particular for rocksalt structure (272 and 155 GPa, respectively). This suggests that the insertion of nitrogen enhances the incompressibility, and may result in a higher hardness. Similar to LaN, among the considered structures, the rocksalt structure is the hardest due to its largest bulk modulus, shear modulus and Young's modulus, and the smallest Poisson's ratio.

TaN: From Table 3, all the considered structures are thermodynamically stable. Different from LaN and HfN, in which the rocksalt structure is the most stable, in TaN, WC structure is the most stable. The second stable structure is NiAs, while rocksalt structure is the third one. For rocksalt structure, our calculated formation enthalpy −1.95 eV is close to the previous GGA result −1.70 eV [28], but differs significantly from the LDA result −2.48 eV [28]. The calculated lattice parameter 4.395 Å deviates by around 2% from the experimental values [14–17,22]. For WC structure, the calculated lattice parameters 2.922 and 2.865 Å are in excellent agreement with the observed values [17–19]. They match each other within 0.2% for *a*-axis and 0.5% for *c*-axis. Although the calculated bulk modulus is in agreement with the previous studies, the calculated elastic stiffness constants do show larger deviation compared to previous theoretical studies (Table 3). On the other hand, the calculated elastic stiffness constants also indicate that only wurtzite structure is mechanically unstable. The most stable structure WC has also the largest bulk modulus 384 GPa, shear modulus 261 GPa, Young's modulus 638 GPa and the smallest Poisson's ratio 0.22. The value 384 GPa is comparable with that of cBN, which is 382 GPa [72] and known as the second superhard material. The calculated bulk modulus ranging from 280 to 384 GPa for all the considered structures is also larger than 200 GPa for the pure metal Ta. In addition, TaN in WC structure will be harder than the ground state of LaN and HfN. This is because the bulk and shear moduli in TaN at WC structure

Table 3
TaN

	NaCl *Fm*-3*m* rocksalt	ZnS *F*-43*m* zinc-blende	CsCl *Pm*-3*m*	ZnS $P6_3mc$ wurtzite	NiAs $P6_3/mmc$	WC *P*-6*m*2	bcc Ta
ΔH	−1.95 −1.70[a], −2.48[b]	−1.53	−1.13	−1.29	−2.31	−2.73	
a	4.395 4.42[a,d], 4.37[b], 4.33[e,f,g] 4.3363[h,i], 4.408[j], 4.40[k], 4.338[m], 4.427[n]	4.734	2.731	3.435	2.895	2.922 2.934[h] 2.938[l], 2.93[o]	3.30[c]
c				5.173	5.836	2.865 2.880[h,o] 2.868[l]	
V	21.2	26.5	20.4	26.4	21.2	21.2	
Ta–N	2.197	2.050	2.365	2.036	2.219	2.213	
C_{11}	881 675.95[d], 886.90[e], 783[q]	318	1006		508	672	260.23[p]
C_{33}					890	911	
C_{44}	74 266.92[d], 355.86[e], 20[q]	22	107		331	287	82.55[p]
C_{12}	122 154.48[d], 162.33[e], 167[q]	261	33		394	256	154.46[p]
C_{13}					172	179	
B	375 338[a], 378[b], 328.3[d] 403.85[e], 329[j], 372[q]	280	357	280	373	384	190[r] 200[c]
G	153	24	208		167	261	69[r]
E	404	71	522		437	638	185[r]
v	0.32	0.46	0.26		0.31	0.22	0.34[r]

For detailed expressions, see Table 1.
[a] Ref. [28], FLAPW method within GGA.
[b] Ref. [28], FLAPW method within LDA.
[c] Refs. [62,63], experiment.
[d] Ref. [36], FLAPW+lo method within GGA.
[e] Ref. [36], FLAPW+lo method within LDA.
[f] Ref. [29], KKR method.
[g] Ref. [15], experiment.
[h] Ref. [17], experiment.
[i] Ref. [14], experiment.
[j] Ref. [35], US-PP within GGA.
[k] Ref. [37], APW method within HL.
[l] Ref. [18], experiment.
[m] Ref. [16], experiment.
[n] Ref. [22], experiment.
[o] Ref. [19], experiment.
[p] Ref. [64], experiment.
[q] Ref. [31], DFPT.
[r] Present work, calculated from the Voigt–Reuss–Hill approximations based on the elastic stiffness constants.

(384 and 261 GPa) are larger than those in LaN (115 and 77 GPa, Table 1) and in HfN (272 and 155 GPa, Table 2) at rocksalt structure. TaN in CsCl structure is also a potential candidate to be hard because of the large shear modulus (208 GPa).

WN: Data on WN are much less than on LaN, HfN and TaN. Experimental studies were only available for rocksalt [73] and WC [19] structures. The calculated formation enthalpy indicates that they are all thermodynamically unstable because of the positive formation enthalpy (Table 4). Among the considered structures, NiAs structure is energetically the most stable, followed by WC and zinc blende structures. Therefore, high temperature and/or high pressure will be necessary for the experimental synthesis. From the previous experimental studies, it is indeed noted that bulk WN in WC structure was synthesized at temperatures between 600 and 800 °C [19]. The thin film of WN in rocksalt structure was prepared at temperatures 723–923 K and pressure 30 Pa [73]. From Table 4, it is seen that the calculated lattice parameter 4.446 Å in rocksalt structure show a slightly large deviation (6%) from the experimental value 4.154 Å [73], but close to 4.35 Å (deviating by 2%) from the previous GGA calculation [35]. For WC structure, the calculated lattice parameters 2.922 and 2.915 Å are in good agreement (deviating by 1% in *a*-axis and 3% in *c*-axis) with the experimental values 2.89 and 2.83 Å [19]. The calculated elastic stiffness constants indicate that only NiAs and WC structures are mechanically stable. The calculated bulk modulus 349 GPa and shear modulus 211 GPa at NiAs structure are larger than or equal to the corresponding values at WC structure and pure metal W. In addition, it is also noticed that the difference of the bulk modulus between the nitride and pure metal decreases from LaN, HfN, TaN to WN. The hardest structures for LaN, HfN, TaN and WN are also the most stable.

ReN: From ReN to AuN (except platinum nitride), we are not aware of any experimental studies on these binary nitrides and only few theoretical studies are found in the literature.

From Table 5, it is noted that only wurtzite structure is thermodynamically stable because of the negative heat of formation (−0.29 eV). Of course, it is also the most stable structure among the considered structures. From the calculated elastic stiffness constants, only wurtzite, NiAs and CsCl structures are mechanically stable. At NiAs structure, it is noted that the calculated bulk modulus 418 GPa is the largest among all the considered structures from LaN to AuN (Tables 1–9). It is also larger than 372 GPa for the pure metal Re and 382 GPa for cBN [72], next to 428 GPa for IrN_2 [74] and 442 GPa for diamond. The relatively larger shear modulus 238 GPa also indicates that ReN in NiAs structure is a potential candidate to be superhard. Since the positive formation energy (0.29 eV) indicates that ReN in NiAs structure cannot be synthesized at ambient conditions, further

Table 4
WN

	NaCl *Fm*-3*m* rocksalt	ZnS *F*-43*m* zinc-blende	CsCl *Pm*-3*m*	ZnS $P6_3mc$ wurtzite	NiAs $P6_3/mmc$	WC *P*-6*m*2	bcc W
ΔH	1.62	0.63	2.33	0.80	0.47	0.62	
a	4.446 4.35[b], 4.20[c], 4.36[d] 4.154[f]	4.730	2.772	3.535	2.913	2.922 2.89[e]	3.16[a]
c				4.721	5.839	2.915 2.83[e]	
V	22.0	26.5	21.3	25.6	21.5	21.6	
W–N	2.223	2.048	2.401	2.057	2.227	2.230	
C_{11}					576	610	522.39[g]
C_{33}					720	712	
C_{44}					238	85	160.83[g]
C_{12}					217	189	204.37[g]
C_{13}					218	214	
B	319 354[b], 394[d]	271	306	236	349	349	310[h] 323[a]
G					211	148	160[h]
E					526	390	410[h]
v					0.25	0.31	0.28[h]

For detailed expressions, see Table 1.
[a] Refs. [62,63], experiment.
[b] Ref. [35], US-PP within GGA.
[c] Ref. [37], APW method with HL.
[d] Ref. [38], PW-PP within LDA.
[e] Ref. [19], experiment.
[f] Ref. [73], experiment.
[g] Ref. [64], experiment.
[h] Present work, calculated from the Voigt–Reuss–Hill approximations based on the elastic stiffness constants.

Table 5
ReN

	NaCl *Fm*-3*m* rocksalt	ZnS *F*-43*m* zinc-blende	CsCl *Pm*-3*m*	ZnS $P6_3mc$ wurtzite	NiAs $P6_3/mmc$	WC *P*-6*m*2	hcp Re
ΔH	1.61	0.51	1.98	-0.29	0.29	0.85	
a	4.297 4.113[c], 4.31[d]	4.569	2.679	2.750	2.759	2.748	2.76[a,b]
c				6.641	5.842	3.005	4.46[a,b]
V	19.8	23.8	19.2	21.7	19.3	19.6	
Re–N	2.148	1.978	2.320	2.034	2.161	2.185	
C_{11}			900	562	727		618.2[e]
C_{33}				777	852		683.5[e]
C_{44}			128	106	216		160.6[e]
C_{12}			122	233	247		275.3[e]
C_{13}				206	245		207.8[e]
B	396 396[d]	310	382	349	418	398	367[f] 372[a,b]
G			204	151	238		178[f]
E			519	396	599		461[f]
v			0.27	0.31	0.26		0.29[f]

For detailed expressions, see Table 1.
[a] Ref. [62], experiment.
[b] Ref. [63], experiment.
[c] Ref. [24], LMTO method.
[d] Ref. [38], PW-PP method within LDA.
[e] Ref. [64], experiment.
[f] Present work, calculated from the Voigt–Reuss–Hill approximations based on the elastic stiffness constants.

study is conducted by applying the pressure (Fig. 4). It is seen that NiAs ($P6_3/mmc$) and CsCl (*Pm*-3*m*) structures become thermodynamically stable at above 5 and 45 GPa, respectively. Wurtzite structure is thermodynamically the most stable when the pressure is less than 42 GPa. Above 42 GPa, the most interesting NiAs structure becomes the most stable. Recalling that recently, PtN_2 [51], IrN_2 [51,74] and OsN_2 [74] have been synthesized by laser-heated diamond anvil cell technique with temperature exceeding 2000 K and pressure around 50 GPa. Thus, ReN in wurtzite and NiAs structures could be synthesized by use of the same experimental conditions.

OsN: Among the transition metals, osmium has the highest bulk modulus (see Table 6 for details). The studies on the pure metal Os are also the recent focus [65–67]. Although OsN_2 has been synthesized recently [74], the study on OsN is far and few between and no experimental report is available on OsN.

From Table 6, the calculated lattice parameter 4.327 Å in rocksalt structure is quite close to 4.335 Å from previous GGA calculation [39]. For WC structure, the calculated parameters are also in reasonable agreement with the previous GGA calculation [39]. Among the considered structures, wurtzite is the most stable. It is also the only one that is mechanically stable.

Table 6
OsN

	NaCl *Fm*-3*m* rocksalt	ZnS *F*-43*m* zinc-blende	CsCl *Pm*-3*m*	ZnS $P6_3mc$ wurtzite	NiAs $P6_3/mmc$	WC *P*-6*m*2	hcp Os
ΔH	2.55	0.79	2.87	0.46	1.69	2.12	
a	4.327 4.058[d], 4.32[e] 4.335[f]	4.565	2.698	2.745	2.777	2.734 2.743[f]	2.74[a,b], 2.5907[c] 2.731[g]
c				6.653	5.901	3.105 3.100[f]	4.32[a,b], 4.1161[c] 4.318[g]
V	20.3 20.37[f]	23.8	19.6	21.7	19.7	20.1 20.186[f]	13.749[h]
Os–N	2.164	1.977	2.337	2.024	2.179	2.214	
C_{11}				651			769.4[g]
C_{33}				788			843.5[g]
C_{44}				139			259.1[g]
C_{12}				162			226.8[g]
C_{13}				144			247.6[g]
B	337 372[e], 342[f]	301	348	331	369	 367[f]	423[k] 418[a,b], 462[c] 424[g], 444.8[h] 411[i], 382.3[j]
G				204			268[k]
E				507			665[k]
v				0.24			0.24[k]

For detailed expressions, see Table 1.
[a] Ref. [62], experiment.
[b] Ref. [63], experiment.
[c] Ref. [65], experiment.
[d] Ref. [24], LMTO method.
[e] Ref. [38], PW-PP method within LDA.
[f] Ref. [39], US-PP method within GGA.
[g] Ref. [66], US-PP method within GGA and LDA.
[h] Ref. [65], full-potential LMTO method within LDA.
[i] Ref. [67], experiment.
[j] Ref. [67], US-PP method within GGA.
[k] Present work, calculated from the Voigt–Reuss–Hill approximations based on the elastic stiffness constants.

Table 7
IrN

	NaCl *Fm*-3*m* rocksalt	ZnS *F*-43*m* zinc-blende	CsCl *Pm*-3*m*	ZnS $P6_3mc$ wurtzite	NiAs $P6_3/mmc$	WC *P*-6*m*2	fcc Ir
ΔH	2.44	1.12	3.15	1.10	1.99	2.74	
a	4.396 4.074[c]	4.636	2.748	2.847	3.083	2.833	3.84[a,b]
c				6.565	5.198	3.085	
V	21.2	24.9	20.7	23.0	21.4	21.4	
Ir–N	2.198	2.008	2.380	2.060	2.204	2.248	
C_{11}		311		292			580[d]
C_{33}				669			
C_{44}		43		88			256[d]
C_{12}		271		256			242[d]
C_{13}				158			
B	322	284	326	253	314		355[e] 355[a,b]
G		31		60			216[e]
E		91		167			540[e]
v		0.44		0.39			0.25[e]

For detailed expressions, see Table 1.
[a] Ref. [62], experiment.
[b] Ref. [63], experiment.
[c] Ref. [24], LMTO method.
[d] Ref. [64], experiment.
[e] Present work, calculated from the Voigt–Reuss–Hill approximations based on the elastic stiffness constants.

The calculated bulk modulus 331 GPa is less than that in pure metal Os and 358 GPa in OsN_2 [74].

IrN: IrN_2 has been recently synthesized and the obtained bulk modulus is 428 GPa [74]. The previous theoretical study gave a bulk modulus of 354 GPa (GGA-PBE) and 392 GPa (LDA-CAPZ) [70], which are less than the experimental value 428 GPa. In addition, IrN_3 was also predicted to be a potential candidate for superhard with bulk modulus 339 GPa (GGA-PBE) and 377 GPa (LDA-CAPZ) [70]. For IrN, only one theoretical study is available and only the lattice parameter was reported [24]. From Table 7, it is seen that the wurtzite structure is the most stable, followed by zinc blende structure. Both structures are the only two that are

Table 8
PtN

	NaCl *Fm*-3*m* rocksalt	ZnS *F*-43*m* zinc-blende	CsCl *Pm*-3*m*	ZnS $P6_3mc$ wurtzite	NiAs $P6_3/mmc$	WC *P*-6*m*2	fcc Pt
ΔH	2.43	1.97	3.41	1.85	2.34	2.95	
a	4.484	4.776	2.814	3.007	3.082	3.027	3.92[a]
	4.137[b], 4.518[c]	4.804[c], 4.779[d], 4.801[e]	2.818[d]	3.040[d]			
	4.491[d], 4.521[e]	4.8041[f], 4.80[g], 4.794[h]					
	4.50[g], 4.504[h]	4.8250[i], 4.780[j]					
c				6.614	5.552	2.957	
				6.606[d]			
V	22.5	27.2	22.3	25.9	22.8	23.5	
Pt–N	2.242	2.068	2.437	2.045	2.256	2.289	
	2.261[e]	2.079[e], 2.080[f]					
C_{11}	296	193		188			346.7[k]
	355[l]	184.1[i], 210[l]					
C_{33}				340			
C_{44}	43	21		16			76.5[k]
	36[l]	13.5[i], 14[l]					
C_{12}	236	217		65			250.7[k]
	248[l]	202.4[i], 241[l]					
C_{13}				100			
B	256	209	254	124	241	226	283[m]
	215.7[c], 229.76[d]	185.5[c], 190.61[d], 187[e]	234.88[d]	99.41[d]			278[a]
	219[e], 230[g]	372[f], 190[g], 192[h]					
	226[h]	196.3[i], 194[j]					
G	37			39			63[m]
E	105			107			177[m]
v	0.43			0.36			0.44[m]

For detailed expressions, see Table 1.
[a] Refs. [62,63], experiment.
[b] Ref. [24], LMTO method.
[c] Ref. [41], fully relativistic FLAPW within GGA.
[d] Ref. [47], augmented plane wave plus lo (APW+lo) method within GGA.
[e] Ref. [42], linear combination of atomic orbitals-crystal orbital (LCAO-CO) method within GGA.
[f] Ref. [23], experiment.
[g] Ref. [46], US-PP method within GGA.
[h] Ref. [43], US-PP method within GGA.
[i] Ref. [44], US-PP method within GGA.
[j] Ref. [45], US-PP method within GGA.
[k] Ref. [64], experiment.
[l] Ref. [43], US-PP method within LDA.
[m] Present work, calculated from the Voigt–Reuss–Hill approximations based on the elastic stiffness constants.

Table 9
AuN

	NaCl *Fm*-3*m* rocksalt	ZnS *F*-43*m* zinc-blende	CsCl *Pm*-3*m*	ZnS $P6_3mc$ wurtzite	NiAs $P6_3/mmc$	WC *P*-6*m*2	fcc Au
ΔH	3.17	3.23	3.89	3.19	3.23	3.54	
A	4.678	4.993	2.913	3.305	3.258	3.180	4.08[a]
	4.662[b]	4.984[b]	2.915[b]	3.600[b]			
	4.541[c]	4.856[c]	2.831[c]	3.45[c]			
C				6.338	5.687	3.000	
				5.75[b], 5.53[c]			
V	25.6	31.1	24.7	30.0	26.1	26.3	
Au–N	2.339	2.162	2.523	2.112	2.358	2.371	
C_{11}	204		278	103			192.44[d]
C_{33}				300			
C_{44}	25		6	9			42.0[d]
C_{12}	162		131	82			162.98[d]
C_{13}				146			
B	176	134	180	102	170	159	173[a,e]
	163.13[b]	118.91[b]	162.58[b]	133.6[b]			
	223.42[c]	161.75[c]	225.66[c]	160.20[c]			
G	23		21	12			28[e]
E	66		61	36			79[e]
v	0.44		0.44	0.44			0.42[e]

For detailed expressions, see Table 1.
[a] Refs. [62,63], experiment.
[b] Ref. [53], FLAPW+lo method within GGA.
[c] Ref. [53], FLAPW+lo method within LDA.
[d] Ref. [64], experiment.
[e] Present work, calculated from the Voigt–Reuss–Hill approximations based on the elastic stiffness constants.

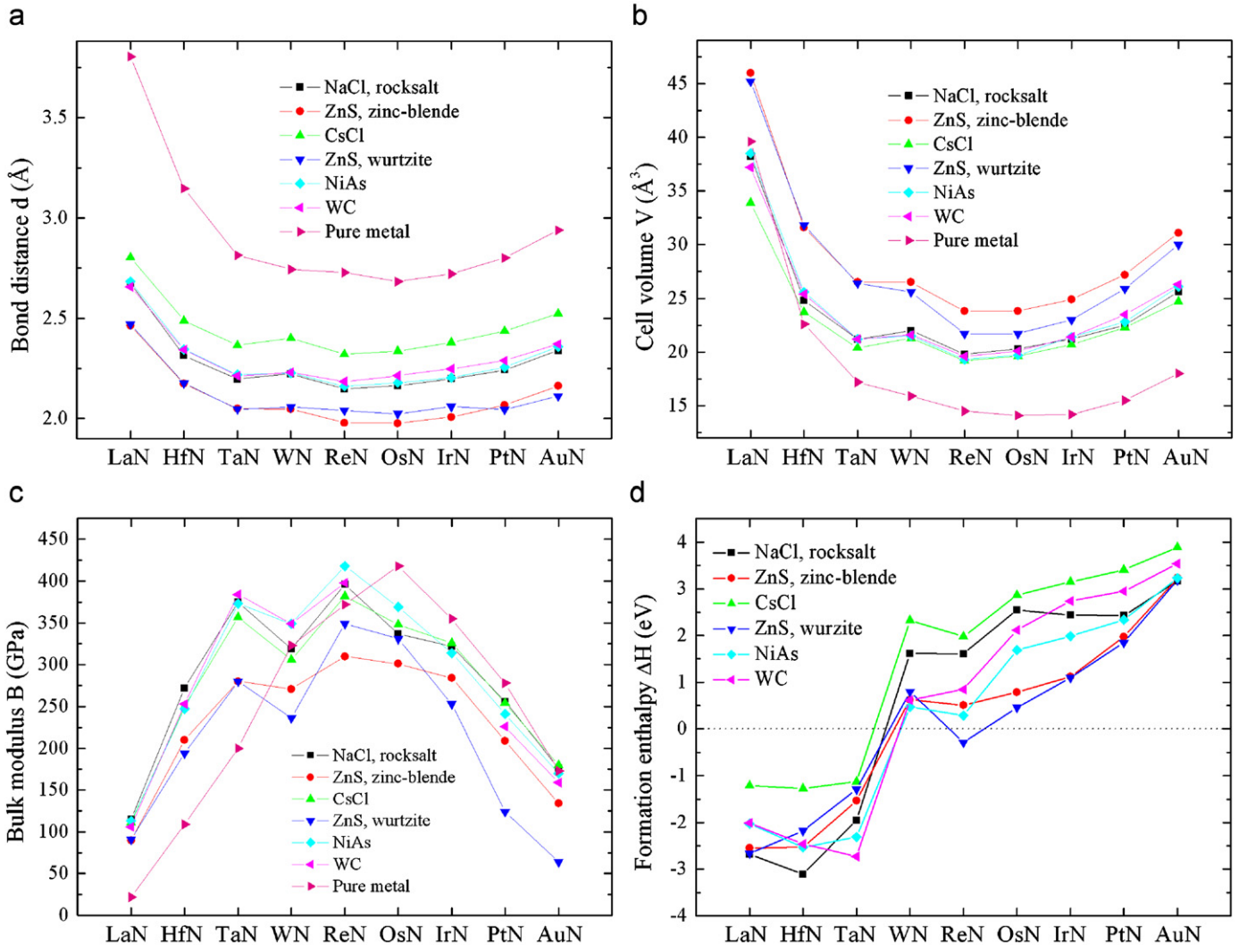

Fig. 2. (Color online) The calculated (a) *M*–N bond distance *d* (Å), (b) volume per formula unit *V* (Å^3), (c) bulk modulus *B* (GPa), and (d) formation enthalpy per formula unit Δ*H* (eV) for all the considered structures of 5*d* transition metal nitrides *M*N (*M* = La–Au) and elemental 5*d* *M* (*M* = La–Au).

mechanically stable. The bulk modulus from the two mechanically stable structures (284 GPa in zinc blende and 253 GPa in wurtzite) are much smaller than 355 GPa for the pure metal Ir.

PtN: As mentioned in the Introduction, PtN has been studied extensively, in particular for rocksalt and zinc blende structures. In this paper, for clarity, only GGA results from the previous studies are selected for PtN; LDA results are not listed. From Table 8, it is seen that compared with previous theoretical studies from the GGA method, the calculated lattice parameters and elastic constants are reasonable. Wurtzite structure is the most stable among the considered structures, followed by zinc blende structure. This is in agreement with the previous theoretical study that wurtzite structure is the most stable among the wurtzite, zinc blende, rocksalt and CsCl structures for PtN [47]. This is also similar to ReN, OsN and IrN, in which wurtzite structure is the most stable. Mechanically stable structures are found for wurtzite and rocksalt structures. Rocksalt structure gives the largest bulk modulus 256 GPa among the considered structures. It is slightly less than 278 GPa for pure metal Pt (Table 8). The small shear modulus 37 GPa reveals that PtN in rocksalt structure is soft.

AuN: Only one theoretical study is available for AuN. From Table 9, it can be seen that the calculated lattice parameter 4.678 Å for rocksalt structure is in good agreement with the previous GGA result 4.662 Å [53]. It also applies to zinc blende and CsCl structures. For wurtzite structure, however, the deviation is slightly larger. Our calculated value 3.305 Å is 9% smaller than the previous GGA result 3.600 Å [53]. Although rocksalt structure is found to be the most stable among the considered structures, the relative energy difference is small. For instance, the energy of the least stable CsCl structure is only 0.72 eV higher than the most stable rocksalt structure. While for other nitrides from LaN to PtN, the relative energy difference is large (see also Fig. 2d). From previous theoretical study, it is also known that rocksalt structure is the most stable among the rocksalt, zinc blende, CsCl and wurtzite structures for AuN [53], in agreement with our prediction. Mechanical stability was found for rocksalt, CsCl and wurtzite structures. The bulk modulus 176 GPa from the most stable rocksalt structure is comparable to 173 GPa for pure metal Au. Finally, it is interesting to note that all the ground state structures from LaN to AuN are mechanically stable structures, as seen from Tables 1 to 9.

3.2. Trends of bonding properties from LaN to AuN

The *M*–N bond distance and cell volume per formula unit for the considered structures of 5*d* transition metal nitrides *M*N (*M* = La–Au) and pure metals *M* (*M* = La–Au) are shown in Fig. 2a

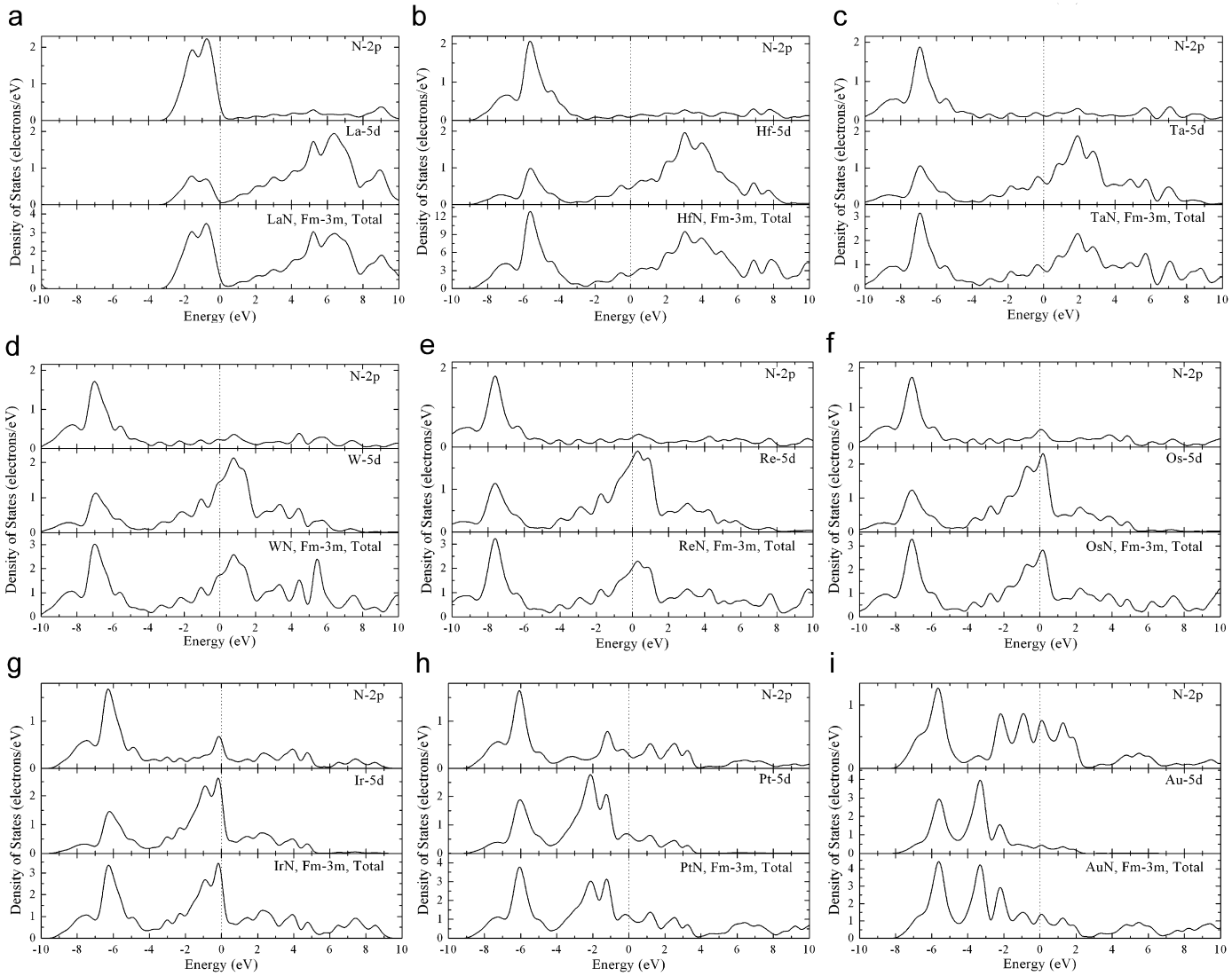

Fig. 3. Total and partial density of states for 5*d* transition metal nitrides with rocksalt structure (*Fm*-3*m*, no. 225) at GGA level. The vertical dotted line at zero indicates the Fermi energy level.

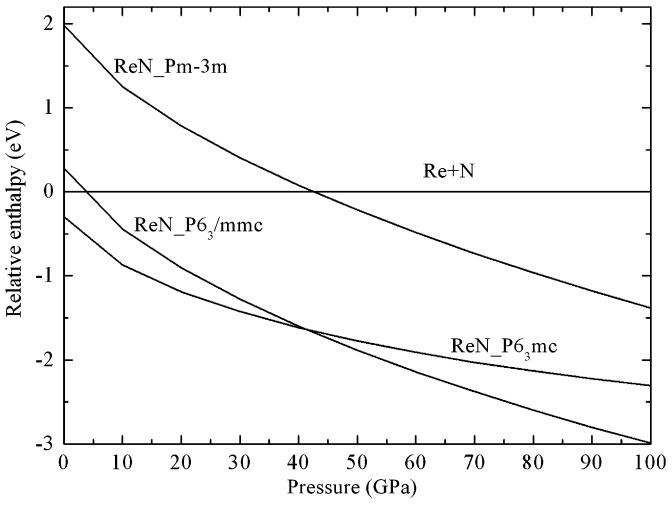

Fig. 4. Enthalpy–pressure diagram for *Re*N at the space groups *Pm*-3*m* (CsCl), *P*6$_3$/*mmc* (NiAs) and *P*6$_3$*mc* (wurtzite) compared with the initial reactants *Re*+N from the GGA calculation.

and b, respectively. From Fig. 2a, it is seen that for all the considered structures, the bond distance decreases from LaN and reaches minimum at *Re*N, and then increases. A similar trend is also observed for the cell volume per formula unit (Fig. 2b). In addition, we also note a slight rise at WN for both bond distance and cell volume. For each nitride, the *M*–N bond distance increases in the following order: zinc blende, wurtzite, rocksalt, NiAs, WC, CsCl and pure metal. From previous theoretical study on 4*d* transition nitride YN, ZrN and NbN with zinc blende and rocksalt structures, it was also found that zinc blende gives shorter *M*–N bond distance than rocksalt structure [7]. In fact, a careful checking on Fig. 2a shows that the *M*–N bond distances can be divided into three groups according to the coordination number of metal atom: (1) the *M*–N bond distances of zinc blende and wurtzite structures with the coordination number of 4 (tetrahedral) for metal atom are the shortest and they are quite close to each other; (2) the bond distances of rocksalt, NiAs and WC structures with the coordination number of 6 for the metal atom are longer than those of zinc blende and wurtzite structures and they are also grouped together; (3) the bond distances of CsCl with the coordination number of 8 for the metal atom are the

longest ones and they form a group by themselves. This indicates that the *M*–N bond distances are closely related to the coordination number of metal atom. As expected, larger coordination number tends to give a longer bond distance. For the cell volume shown in Fig. 2b, only two groups can be found: (1) the volumes of zinc blende and wurtzite structures are relatively large; (2) the volumes of the remaining four structures are relatively small. The smaller cell volume of rocksalt structure than that of zinc blende structure is also observed in 4*d* transition metal nitrides [7]. The volume change between rocksalt and zinc blende structures might be explained by the fact that the nitrogen atoms are inserted at the octahedral sites in the rocksalt structure, which brings a smaller lattice expansion than the tetrahedral sites of nitrogen atoms in the zinc blende structure.

Compared with rocksalt and zinc blende 3*d* [3,4] and 4*d* [5–7] nitrides, it is not surprising to see that the corresponding lattice parameters of 5*d* nitrides (Tables 1–9) are larger than those of 3*d* and 4*d* nitrides. With the increase of atomic number, the lattice parameters also show the same trend, i.e., the lattice parameters decrease initially, reach the minimum at the middle of the series and then increase.

In addition, the bond distances of pure metals are longer than those of the corresponding nitrides, while the volumes of pure metals are smaller than those of the corresponding nitrides. This may be explained by the fact that the coordination number of metals La, Hf, Re, Os, Ir, Pt and Au is 12, while that of Ta and W is 8, larger than those of the corresponding nitrides.

The bulk modulus for the considered structures is shown in Fig. 2c, in which the bulk modulus of OsN and IrN in WC structure is not presented due to failure in calculating the quantity. From Fig. 2c, as expected, the bulk modulus shows the opposite behavior compared with the *M*–N bond distance and cell volume. On going from LaN to AuN, the bulk modulus increases initially, reaches the maximum at *Re*N (except for a slight drop at WN), then decreases. The drop at WN is due to the rise in the cell volume (Fig. 2b). Similar trend is observed for pure metals, but the maximum is shifted to osmium. From previous studies on zinc blende 4*d* nitrides, it is also noticed that the bulk modulus shows the same trend with the maximum at TcN [7]. While for pure metals, the maximum is at Ru [7]. On the other hand, for LaN, HfN and TaN, their corresponding bulk modulus are larger than that of pure metals La, Hf and Ta, respectively. For WN and *Re*N, the bulk modulus of pure metal is among the considered structures, while for OsN, IrN, and PtN, the bulk modulus is less than that of the pure metals. For AuN, the bulk modulus of pure metal is close to the largest bulk modulus among the considered structures. Zinc blende and wurtzite structures with the tetrahedral unit have relatively smaller bulk modulus, followed by the CsCl structure. Rocksalt, NiAs and WC structures with the coordination number of 6 for metal atom have relatively larger bulk modulus. Similar to 5*d* transition metal carbides [38], the larger bulk modulus for the nitride from LaN to ReN indicates that the directional (covalent) bonding and large charge density are formed between 5*d* metal and nitrogen (as shown in the DOS discussed below). From Os to Au, strong directional bonding is formed for pure metals, and no advantage is gained by the addition of nitrogen.

The formation enthalpy per formula unit for the considered structures was shown in Fig. 2d. It is seen that the general trend of the formation enthalpy increases from LaN to AuN. The increase of formation enthalpy coincides with the fact that the bonding strength decreases from LaN to AuN (for the bonding behavior between metal 5*d* and N 2*p* states, see later section). For rocksalt structure, the trend in our calculation is the same as that from the previous study on the 5*d* transition metal nitrides (from LaN to PtN) [24,25]. Similar trend was also observed in 3*d* and 4*d* nitrides in rocksalt structure [25]. A rise in formation enthalpy was observed for WN, as in the *M*–N bond distance and cell volume (Fig. 2a and b), in particular for wurtzite, NiAs and CsCl structures. For LaN, HfN and TaN, the formation enthalpy is negative for the structures considered. This suggests the all the considered structures can be synthesized at ambient conditions for the three nitrides. From WN to AuN, except wurtzite structure in *Re*N, the formation enthalpy is positive. This indicates the high temperature and/or high pressure are/is necessary for the synthesis of the considered structures. Among the considered structures, rocksalt structure is the most stable for LaN, HfN and AuN, and so is WC for TaN, NiAs for WN, wurtzite for ReN, OsN, IrN and PtN. For the most studied rocksalt and zinc blende structures, it is interesting to note that the formation enthalpy of zinc blende structure is higher than that in rocksalt structure from LaN to TaN and lower from WN to AuN (Fig. 2d). CsCl structure is the least stable among the considered structures due to the largest formation enthalpy.

Due to the similarity of the total and partial DOS for the considered structures, only the DOS for rocksalt structure are shown in Fig. 3. DOS for the other considered structures are given in the Supplementary materials (Figs. S1–S5). It is seen that metallic behavior is obtained for all the considered structures in each 5*d* nitride due to the finite DOS at the Fermi energy level.

In rocksalt structure, it is seen that except the LaN, the DOS can be divided into three regions: (1) from −10 to −4 eV, the DOS is composed of the contribution from metal 5*d* and N 2*p* states, which have a strong hybridization; (2) from −4 to 0.0 eV, the contribution is mainly from the metal 5*d* states, with small or negligible N 2*p* states; (3) above the Fermi energy level, the contribution is from the unoccupied 5*d* states. With the increase in atomic number, the character of *d* states becomes obvious around the Fermi energy level. In LaN, the bonding 5*d* states locates at the energy region from −3.0 to 0.0 eV. Upon increasing one electron in HfN, the 5*d* states shift significantly and extend from −9.0 to 0.0 eV. From TaN to OsN, the 5*d* states and N 2*p* states are very dispersive. From IrN to AuN, both 5*d* states and N 2*p* states become localized again. Similar trend is also observed for other structures shown compared to those given in the Supplemental materials (Figs. S1 to S5), i.e., the dispersive 5*d* states are observed in the middle of the series. After a careful checking of Fig. 3 and Figs. S1–S5, it is also noted that for zinc blende (Fig. S1) and wurtzite (Fig. S3) structures with tetrahedral unit, the extent of dispersion is smaller than that of rocksalt (Fig. 3), WC (Fig. S4), NiAs (Fig. S5) structures with the coordination number of 6 for metal atom and CsCl (Fig. S2) with the coordination number of 8. Comparing with the *M*–N bond distances (Fig. 2a), it is seen that the relatively short bond distances correspond to the dispersive 5*d* states. This indicates that the width of 5*d* states is closely related to the bond distances. If the bond distance is increased, the hybridization of 5*d* states with N 2*p* states will be reduced. That is, the width of 5*d* states will be decreased, and 5*d* electrons will tend to be localized. If the bond distance is decreased, the 5*d* states will tend to be dispersive. The strong hybridization between 5*d* states and N 2*p* states for the considered structures reveals that the bonding between 5*d* metal and N is mainly covalent.

From the previous study on the rocksalt 3*d* transition metal mononitrides [75], it is known that only the bonding states are filled for ScN with 8 valence electrons per formula unit. For valence electrons per formula unit from 9 in TiN to 12 in MnN, the additional electrons will occupy the non-bonding states. This does not modify the bonding properties significantly, but does make the compound metallic. For valence electrons from 13 in FeN to 18 in ZnN, the anti-bonding states will be occupied. This makes the rocksalt structure energetically unfavorable. The bond distance will be enlarged and cohesion will be reduced [75]. From our calculated DOS for rocksalt structure (Fig. 3), it is clear that the above conclusions obtained for 3*d* transition metal nitrides also apply to the 5*d* transition metal nitrides. From Fig. 3, for LaN with

8 valence electrons per formula unit, the bonding between La 5*d* and N 2*p* states is clearly seen in the region from −3.0 to 0.0 eV. By adding an extra electron, non-bonding state appears in HfN with 9 valence electrons in the region from −3.0 to 0.0 eV because 5*d* states are dominant in that region, while nearly no contribution occurs from the N 2*p* states. The non-bonding state continues till *Re*N. From OsN with 13 valence electrons, the anti-bonding state starts to appear due to the involvement of the N 2*p* states. Although the above phenomenon was obtained for rocksalt structure, similar behavior was also observed for other structures considered (Figs. S1–S5). In addition, due to the filling of the anti-bonding states, the calculated *M*–N bond distances (Fig. 2a) increase from OsN with 13 valence electrons to AuN with 16 valence electrons, in agreement with those obtained in the 3*d* transition metal mononitrides [75]. In addition, the filling of the anti-bonding states also make the localization of DOS from OsN to AuN, as reported for 3*d* transition metal nitrides [75].

4. Conclusions

5*d* transition metal mononitrides from LaN to AuN were studied by the density-functional method. Six structures are considered for each nitride, i.e., rocksalt, zinc blende, CsCl, wurtzite, NiAs and WC structures. Our calculation shows that metal and nitrogen bond distances *M*–N are closely related to the coordination number of metal atom. Larger coordination number tends to give a longer bond distance. The *M*–N bond distance decreases initially and reaches minimum at *Re*N, and then increases. Similar trend applies to the cell volume. For the calculated bulk modulus, it increases initially, reaches the maximum at *Re*N, then decreases. The formation enthalpy tends to increase from LaN to AuN. Among the considered structures, rocksalt structure is the most stable for LaN, HfN and AuN, and so is WC structure for TaN, NiAs structure for WN, wurtzite structure for *Re*N, OsN, IrN and PtN. The most stable structure for each nitride is mechanically stable. For LaN, HfN and TaN, the formation enthalpy is negative for all the structures considered, while from WN to AuN, except wurtzite structure in *Re*N, the formation enthalpy is positive. The negative formation enthalpy indicates that the compound can be synthesized at ambient conditions. Among all the considered structures, covalent behavior was observed for metal–nitrogen bond because of the strong hybridization between metal 5*d* and N 2*p* states. The calculated DOS shows that all the considered structures are metallic. The width of 5*d* states is closely related to the metal–nitrogen bond distances. The long bond distance makes the width of 5*d* states decrease, i.e., 5*d* electrons will tend to be localized. While the short bond distance will make the 5*d* states to be dispersive. Among the mechanically stable structures, *Re*N in NiAs structure has the largest bulk modulus, 418 GPa, followed by 384 GPa for TaN in WC structure. The largest shear modulus 261 GPa is from TaN in WC structure, followed by 238 GPa for *Re*N in NiAs structure. The pressure study indicates that *Re*N in NiAs structure becomes thermodynamically stable above 5 GPa and the most stable above 42 GPa. Therefore, these potential superhard materials, in particular their films, might have potential applications such as hard coating for magnetic storage devices.

Acknowledgment

The authors thank the National Natural Science Foundation of China for financial support (Grant nos. 20773117, 20571073 and 20331030).

Appendix A. Supplementary Materials

Supplementary data associated with this article can be found in the online version at doi:10.1016/j.jssc.2008.07.022.

References

[1] L.E. Toth, Transition Metal Carbides and Nitrides, Academic Press, New York, 1971.
[2] S.T. Oyama (Ed.), The Chemistry of Transition Metal Carbides and Nitrides, Blacklie Academic & Professional, London, 1996.
[3] B. Eck, R. Dronskowski, M. Takahashi, S. Kikkawa, J. Mater. Chem. 9 (1999) 1527.
[4] J. Häglund, G. Grimvall, T. Jarlborg, A.F. Guillermet, Phys. Rev. B 43 (1991) 14400.
[5] A.F. Guillermet, J. Häglund, G. Grimvall, Phys. Rev. B 45 (1992) 11557.
[6] R. de Paiva, R.A. Nogueira, J.L.A. Alves, Braz. J. Phys. 36 (2006) 470.
[7] R. de Paiva, R.A. Nogueira, J.L.A. Alves, Phys. Rev. B 75 (2007) 085105.
[8] U. Essen, W. Klemm, Z. Anorg. Allg. Chem. 317 (1962) 25.
[9] G.L. Olcese, J. Phys. F: Met. Phys. 9 (1979) 569.
[10] A.N. Christensen, Acta Chem. Scand. 44 (1990) 851.
[11] X. Chen, V.V. Struzhkin, Z. Wu, M. Somayazulu, J. Qian, S. Kung, A.N. Christensen, Y. Zhao, R.E. Cohen, H.-K. Mao, R.J. Hemley, Proc. Natl. Acad. Sci. Am. 102 (2005) 3198.
[12] S. Yamanaka, K. Hotehama, H. Kawaji, Nature 392 (1998) 580.
[13] X. Chen, V.V. Struzhkin, S. Kung, H.-K. Mao, R.J. Hemley, A.N. Christensen, Phys. Rev. B 70 (2004) 014501.
[14] T. Mashimo, S. Tashiro, T. Toya, M. Nishida, H. Yamazaki, S. Yamaya, K. Oh-ishi, Y. Syono, J. Mater. Sci. 28 (1993) 3439.
[15] E.K. Molodovskaya, V.F. Petrunin, I. Karimov, M. Karimov, T. Khaydarov, I.P. Borovinskaya, A.N. Pityulin, A.G. Merzhanov, Fiz. Met. Metalloved. 40 (1975) 202.
[16] I.P. Parkin, A.T. Rowley, Adv. Mater. 6 (1994) 780.
[17] T. Mashimo, S. Tashiro, M. Nishida, K. Miyahara, E. Eto, Physica B 239 (1997) 13.
[18] T. Mashimo, S. Tashiro, J. Mater. Sci. Lett. 13 (1994) 174.
[19] N. Schönberg, Acta Metall. 2 (1954) 427.
[20] R. Nowak, C.L. Li, Thin Solid Films 305 (1997) 297.
[21] C. Angelkort, A. Berendes, H. Lewalter, W. Bock, B.O. Kolbesen, Thin Solid Films 437 (2003) 108.
[22] H.B. Nie, S.Y. Xu, S.J. Wang, L.P. You, Z. Yang, C.K. Ong, J. Li, T.Y.F. Liew, Appl. Phys. A 73 (2001) 229.
[23] E. Gregoryanz, C. Sanloup, M. Somayazulu, J. Badro, G. Fiquet, H.-K. Mao, R.J. Hemley, Nat. Mater. 3 (2004) 294.
[24] A.F. Guillermet, J. Häglund, G. Grimvall, Phys. Rev. B 48 (1993) 11673.
[25] J. Häglund, A.F. Guillermet, G. Grimvall, M. Körling, Phys. Rev. B 48 (1993) 11685.
[26] G. Vaitheeswaran, V. Kanchana, M. Rajagopalan, Solid State Commun. 124 (2002) 97.
[27] Y.O. Ciftci, K. Çolakoglu, E. Deligoz, H. Ozisik, Mater. Chem. Phys. 108 (2008) 120.
[28] C. Stampfl, W. Mannstadt, R. Asahi, A.J. Freeman, Phys. Rev. B 63 (2001) 155106.
[29] P. Weinberger, C.P. Mallett, R. Podloucky, A. Neckel, J. Phys. C: Solid State Phys. 13 (1980) 173.
[30] A. Zaoui, B. Bouhafs, P. Ruterana, Mater. Chem. Phys. 91 (2005) 108.
[31] Z. Wu, X. Chen, V.V. Struzhkin, R.E. Cohen, Phys. Rev. B 71 (2005) 214103.
[32] S. Nagao, K. Nordlund, R. Nowak, Phys. Rev. B 73 (2006) 144113.
[33] P. Ojha, M. Aynyas, S.P. Sanyal, J. Phys. Chem. Solids 68 (2007) 148.
[34] E.I. Isaev, R. Ahuja, S.I. Simak, A.I. Lichtenstein, Yu.Kh. Vekilov, B. Johansson, I.A. Abrikosov, Phys. Rev. B 72 (2005) 064515.
[35] E.I. Isaev, S.I. Simak, I.A. Abrikosov, R. Ahuja, Yu.Kh. Vekilov, M.I. Katsnelson, A.I. Lichtenstein, B. Johansson, J. Appl. Phys. 101 (2007) 123519.
[36] M. Sahnoun, C. Daul, M. Driz, J.C. Parlebas, C. Demangeat, Comp. Mater. Sci. 33 (2005) 175.
[37] D.A. Papaconstantopoulos, W.E. Pickett, B.M. Klein, L.L. Boyer, Phys. Rev. B 31 (1985) 752.
[38] J.C. Grossman, A. Mizel, M. Côté, M.L. Cohen, S.G. Louie, Phys. Rev. B 60 (1999) 6343.
[39] J.-C. Zheng, Phys. Rev. B 72 (2005) 052105.
[40] M.B. Kanoun, S. Goumri-Said, Phys. Rev. B 72 (2005) 113103.
[41] B.R. Sahu, L. Kleinman, Phys. Rev. B 71 (2005), 041101(R), 209904(E); B.R. Sahu, L. Kleinman, Phys. Rev. B 72 (2005) 119901(E).
[42] J. Uddin, G.E. Scuseria, Phys. Rev. B 72 (2005), 035101, 119902(E).
[43] S.K.R. Patil, S.V. Khare, B.R. Tuttle, J.K. Bording, S. Kodambaka, Phys. Rev. B 73 (2006) 104118.
[44] C.Z. Fan, L.L. Sun, Y.X. Wang, Z.J. Wei, R.P. Liu, S.Y. Zeng, W.K. Wang, Chin. Phys. Lett. 22 (2005) 2637.
[45] R. Yu, X.F. Zhang, Appl. Phys. Lett. 86 (2005) 121913.
[46] J. von Appen, M.-W. Lumey, R. Dronskowski, Angew. Chem. Int. Ed. 45 (2006) 4365.
[47] L.H. Yu, K.L. Yao, Z.L. Liu, Y.S. Zhang, Physica B 399 (2007) 50.

[48] R. Yu, X.F. Zhang, Phys. Rev. B 72 (2005) 054103.
[49] R. Yu, Q. Zhan, X.F. Zhang, Appl. Phys. Lett. 88 (2006) 051913.
[50] A.F. Young, J.A. Montoya, C. Sanloup, M. Lazzeri, E. Gregoryanz, S. Scandolo, Phys. Rev. B 73 (2006) 153102.
[51] J.C. Crowhurst, A.F. Goncharov, B. Sadigh, C.L. Evans, P.G. Morrall, J.L. Ferreira, A.J. Nelson, Science 311 (2006) 1275.
[52] H. Gou, L. Hou, J. Zhang, G. Sun, L. Gao, F. Gao, Appl. Phys. Lett. 89 (2006) 141910.
[53] M.B. Kanoun, S. Goumri-Said, Phys. Lett. A 362 (2007) 73.
[54] M.D. Segall, P.J.D. Lindan, M.J. Probert, C.J. Pickard, P.J. Hasnip, S.J. Clark, M.C. Payne, J. Phys.: Condens. Matter 14 (2002) 2717.
[55] D. Vanderbilt, Phys. Rev. B 41 (1990) 7892.
[56] H.J. Monkhorst, J.D. Pack, Phys. Rev. B 13 (1976) 5188;
J.D. Pack, H.J. Monkhorst, Phys. Rev. B 16 (1977) 1748.
[57] J.P. Perdew, K. Burke, M. Ernzerhof, Phys. Rev. Lett. 77 (1996) 3865.
[58] J.A. Venables, C.A. English, Acta Crystallogr. Sec. B: Struct. Crystallogr. Cryst. Chem. 30 (1974) 929.
[59] W. Voigt, Lehrburch der Kristallphysik, Teubner, Leipzig, 1928.
[60] A. Reuss, Z. Angew. Math. Mech. 9 (1929) 49.
[61] R. Hill, Proc. Phys. Soc. London 65 (1952) 350.
[62] C. Kittel, Introduction to Solid State Physics, Wiley, New York, 1971.
[63] J. Donohue, The Structures of the Elements, Wiley, New York, 1974, pp. 191–199.
[64] D.R. Lide, CRC Handboook of Chemistry and Physics, 86th ed, CRC Press, Florida, 2005–2006, pp. 12-33–12-37.
[65] H. Cynn, J.E. Klepeis, C.-S. Yoo, D.A. Young, Phys. Rev. Lett. 88 (2002) 135701.
[66] C.Z. Fan, S.Y. Zeng, L.X. Li, Z.J. Zhan, R.P. Liu, W.K. Wang, P. Zhang, Y.G. Yao, Phys. Rev. B 74 (2006) 125118.
[67] F. Occelli, D.L. Farber, J. Badro, C.M. Aracne, D.M. Teter, M. Hanfland, B. Canny, B. Couzinet, Phys. Rev. Lett. 93 (2004) 095502.
[68] F. Hulliger, in: K.A. Gschneider Jr., L.R. Eyring (Eds.), Handbook of Physics and Chemistry of Rare Earths, vol. 4, North-Holland, Amsterdam, 1974, pp. 153–236.
[69] M. Hasegawa, K. Niwa, T. Yagi, Solid State Commun. 141 (2007) 267.
[70] Z.J. Wu, E.J. Zhao, H.P. Xiang, X.F. Hao, X.J. Liu, J. Meng, Phys. Rev. B 76 (2007) 054115, 76 (2007) 059904(E).
[71] R. Heid, K.-P. Bohnen, B. Renker, T. Wolf, H. Schober, Phys. Rev. B 71 (2005) 092302.
[72] E.V. Yakovenko, I.V. Aleksandrov, A.F. Gonchavrov, S.M. Stishov, Sov. Phys. JETP 68 (1989) 1213.
[73] H.-T. Chiu, S.-H. Chuang, J. Mater. Res. 8 (1993) 1353.
[74] A.F. Young, C. Sanloup, E. Gregoryanz, S. Scandolo, R.J. Hemley, H.-K. Mao, Phys. Rev. Lett. 96 (2006) 155501.
[75] W.A. Harrison, G.K. Straub, Phys. Rev. B 36 (1987) 2695.